Hydrol. Earth Syst. Sci. Discuss., 8, 7657–7707, 2011
www.hydrol-earth-syst-sci-discuss.net/8/7657/2011/
doi:10.5194/hessd-8-7657-2011

Hydrology and Earth System Sciences Discussions

Shallow rainwater lenses in deltaic areas with saline seepage

P. G. B. de Louw[1], S. Eeman[2], B. Siemon[3], B. R. Voortman[4], J. Gunnink[5], E. S. van Baaren[1], and G. H. P. Oude Essink[1]

[1]Deltares, Dept. of Soil and Groundwater, P.O. Box 85467, 3508 AL Utrecht, The Netherlands
[2]Wageningen University, Environmental Sciences Group, Soil Physics, Ecohydrology and Groundwater Management, P.O. Box 47, 6700 AA Wageningen, The Netherlands
[3]Federal Institute for Geosciences and Natural Resources, Dept. of Groundwater and Soil Science, Stilleweg 2, 30655 Hanover, Germany
[4]KWR Watercycle Research Institute, P.O. Box 1072, 3430 BB, Nieuwegein, The Netherlands
[5]TNO Geological Survey of the Netherlands, P.O. Box 80015, 3508 TA Utrecht, The Netherlands

Received: 15 July 2011 – Accepted: 26 July 2011 – Published: 10 August 2011

Correspondence to: P. G. B. de Louw (perry.delouw@deltares.nl)

Published by Copernicus Publications on behalf of the European Geosciences Union.

Abstract

In deltaic areas with saline seepage, fresh water availability is often limited to shallow rainwater lenses lying on top of saline groundwater. Here we describe the characteristics and spatial variability of such lenses in areas with saline seepage and the mechanisms that control their occurrence and size. Our findings are based on different types of field measurements and detailed numerical groundwater models applied in the south-western delta of The Netherlands. By combining the applied techniques we could extrapolate in situ measurements at point scale (groundwater sampling, TEC (temperature and electrical soil conductivity)-probe measurements, electrical cone penetration tests (ECPT)) to a field scale (continuous vertical electrical soundings (CVES), electromagnetic survey with EM31), and even to a regional scale using helicopter-borne electromagnetic measurements (HEM). The measurements show a gradual S-shaped mixing zone between infiltrating fresh rainwater and upward flowing saline groundwater. The mixing zone is best characterized by the depth of the centre of the mixing zone D_{mix}, where the salinity is half that of seepage water, and the bottom of the mixing zone B_{mix}, with a salinity equal to that of the seepage water (Cl-conc. 10 to 16 g l^{-1}). D_{mix} manifests at very shallow depth in the confining top layer, on average at 1.7 m below ground level (b.g.l.), while B_{mix} lies about 2.5 m b.g.l. Head-driven forced convection is the main mechanism of rainwater lens formation in the saline seepage areas rather than free convection due to density differences. Our model results show that the sequence of alternating vertical flow directions in the confining layer caused by head gradients determines the position of the mixing zone (D_{mix} and B_{mix}) and that these flow directions are controlled by seepage flux, recharge and drainage depth.

1 Introduction

In many deltaic areas, the groundwater is saline because of sea water intrusion and marine transgressions (Custodio and Bruggeman, 1987; Stuyfzand and Stuurman, 1994; Weert et al., 2009, Post and Abarca, 2010). In areas that lie below mean sea level (b.m.s.l.) or at large geohydrological gradients, saline groundwater may reach the surface by upward groundwater flow. This leads to salinization of surface waters and shallow fresh[1] groundwater bodies and makes the water unfit for irrigation, drinking water supply or industrial purposes (e.g. Van Rees Veilinga et al., 1981; Van den Eertwegh et al., 2006; Giambastiani et al., 2007; De Louw et al., 2010, 2011). A future rise in sea level is expected to increase the seepage and salt loads to surface waters and reduce the availability of both fresh surface water and groundwater (e.g. Meisler et al., 1984; Navoy, 1991; Oude Essink, 1996; Van der Meij and Minnema, 1999; Vandenbohede et al., 2008). Model simulations show that salt loads from groundwater seepage in several low-lying parts of the coastal zone of the Netherlands will be doubled due to sea level rise by 2100 A.D. (Oude Essink et al., 2010).

In contrast to the salt loading process to surface waters by saline groundwater seepage, little attention has so far been given to the interaction of upward flowing saline groundwater with infiltrating rainwater in the topsoil, as illustrated in Fig. 1. The upward movement of saline groundwater prevents rainwater from infiltrating to greater depths, resulting in shallow rainwater lenses (Fig. 1). Under certain conditions the rainwater lens may become so small, or even disappear, that saline groundwater may reach the root zone via capillary rise, affecting crop growth (Steppuhn et al., 2005; Katerji et al., 2003; Flowers, 2004; Rozema and Flowers, 2008) and natural vegetation (Jolly et al., 2008; Antonellini and Mollema, 2009). We suspect that the shallow rainwater lenses in areas with saline seepage are very vulnerable to climate change (changing precipitation surpluses) and to a rising sea level (enhancing seepage) as shown by Maas (2007).

Here we focus on the occurrence of shallow rainwater lenses in areas with saline seepage and the processes involved. So far, research into fresh rainwater lenses in

[1]In this paper, we classify groundwater salinity based on chloride (Cl^-) concentration into fresh ($Cl^- < 0.3\,g\,l^{-1}$), brackish ($>0.3\,g\,l^{-1}$ $Cl^- < 1.0\,g\,l^{-1}$) and salt ($Cl^- > 1.0\,g\,l^{-1}$). Cl^- is the major conservative anion in the coastal plain and subsurface of the Netherlands.

HESSD
8, 7657–7707, 2011

saline groundwater has mainly been focussed on so-called Badon Ghijben-Herzberg (BGH) fresh water lenses in elevated areas like sandy dunes along the coast and on small islands that lack an upward groundwater flow (e.g. Badon Ghijben, 1888; Herzberg, 1901; Fetter, 1972; Van Dam and Sikkema, 1982; Meinardi, 1983; Underwood et al., 1992; Collins and Easley, 1999; Bakker, 2000). Unlike rainwater lenses in seepage areas, BGH-lenses develop under downward vertical head gradients by the infiltration of rainwater into a saline groundwater body. BGH-lenses are generally thick and the depth of the freshwater-saline interface is mainly controlled by the buoyancy force of the denser saline groundwater.

Some analytical and numerical steady-state approaches to modelling rainwater lenses under conditions of upward groundwater seepage have been described (Schot et al., 2004; Maas, 2007; Eeman et al., 2011). Eeman et al. (2011) investigated the parameter groups that dominate the mixing processes for physically feasible ranges of parameters, using the analytical approach by Maas (2007) and the numerical transport code SUTRA (Voss and Provost, 2008). Schot et al. (2004) used a numerical model to simulate the development of rainwater lenses in fens under fresh groundwater seepage conditions. So far, theoretical models for shallow fresh rainwater lenses have not been based on actual observations, since there were no detailed measurements available. In addition, predicting the effects of climate change and sea level rise, and formulating mitigation measures is only meaningful when the current situation of these shallow rainwater lenses is known. We therefore aimed to gain a thorough understanding of the occurrence and characteristics of shallow rainwater lenses on top of seeping saline groundwater.

In this article we determine the characteristics and spatial variability of rainwater lenses in areas with saline seepage on the basis of field measurements and numerical groundwater models, including variable-density groundwater flow and coupled salt transport. Moreover, we determine the main factors that control the characteristics and occurrence of these shallow rainwater lenses. Our study area was the province of Zeeland, situated in the south-western delta of the Netherlands, where saline groundwater

HESSD
8, 7657–7707, 2011

with chloride concentrations exceeding 10 g l^{-1} is found within five meters below ground level (Goes et al., 2009). Different in situ and ex situ field techniques, namely groundwater sampling, TEC (temperature and electrical soil conductivity)-probe measurements, electrical cone penetration tests (ECPT), continuous vertical electrical soundings (CVES), electromagnetic survey with EM31 and helicopter-borne electromagnetic measurements (HEM) were used to map the thickness of these shallow rainwater lenses and the mixing zone from fresh to saline groundwater.

2 Paleogeography, geomorphology and hydrogeology of study area

The study area lies in the south-western delta of the Netherlands (Fig. 2a). The current landscape, groundwater flow systems and groundwater salinity mainly result from sequential Holocene marine transgressions and regressions, and human activities such as peat exploitation and land reclamation. Under a continuous sea level rise during the Holocene, Zeeland was submerged from 7500 B.P. (before present) until 5000 B.P. (Van de Plassche, 1982; Vos and Zeiler, 2008) and the infiltration of sea water salinized the underlying Pleistocene aquifers by free convection (Post, 2004). After this period of maximum transgression, sedimentation processes began to dominate and, as a consequence, the land rose above mean sea level (a.m.s.l.). Then peat was formed under fresh water conditions and this covered Zeeland between 3800 B.P. and 2000 B.P. Since Roman times, peat cutting and dewatering of the land by man has caused subsidence enhanced by marine erosion (Fig. 2b). Zeeland was again totally submerged from 350 A.D. until 750 A.D. (Fig. 2b). Around 1000 A.D. people started to reclaim large pieces of land by the embankment of the salt marshes (supra-tidal flats) (Fig. 2b; Vos and Zeiler, 2008). Such an embanked land which is drained artificially is called a “polder” (Van de Ven, 2003). Shrinkage of peat and clay by drainage and peat cutting led to subsidence of these polders, whereas the unembanked land was rising from sedimentation during high tides and storms (Vos and Zeiler, 2008).

Discussion Paper | Discussion Paper | Discussion Paper | Discussion Paper |

HESSD

8, 7657–7707, 2011

Shallow rainwater lenses in deltaic areas with saline seepage

P. G. B. de Louw et al.

The present topography is therefore a result of the age of reclamation; the older the land, the lower the surface elevation. The lowest polders are situated at −1.5 to −2.5 m b.m.s.l. whereas the more recent polders have their land surface above m.s.l. (Fig. 2c). As the former tidal creeks consisted of sand, they did not subside like the surrounding clayey and peaty salt marshes. The present land surface at these sandy creek ridges is therefore often 0.5 to 1.5 m higher than the surrounding land (Fig. 2c–d). In the western coastal area, sandy dunes were formed during the Holocene that now reach elevations of 30 m a.m.s.l. Taking into account that the present elevation has a large impact on the groundwater flow system, the study area can be divided into three major geomorphic units: (a) reclaimed salt marshes, (b) sandy creek ridges and (c) the dunes (Fig. 2d). Fresh rainwater infiltrates the dunes and the elevated sandy creek ridges, whereas upward groundwater seepage occurs mainly in the low-lying reclaimed salt marshes (Fig. 2e). The salt marshes are intensively drained artificially by a regular system of ditches and tile drainage to make the land fit for agriculture. The ditches lie some 50 to 200 m apart and tile drainage is applied at a depth of about 1 m, with a distance of 10 to 15 m between the drains.

Besides elevation and drainage characteristics, the composition of the Holocene deposits plays an important role in groundwater flow and the formation of shallow fresh rainwater lenses in above the present saline groundwater. Due to the dynamic palaeographical evolution of the study area during the Holocene, the lithological content of the Holocene sediments is fairly heterogeneous. An east-west lithological cross-section of the island of Schouwen-Duivenland shows the general build-up of the Holocene sediments on top of late Pleistocene cover-sands (Fig. 3). In most of the area, the fining upward sequence of the Holocene deposits resulted in a thin confining layer of clay and peat on top of an aquifer of Pleistocene and Holocene fine to coarse sands (upper aquifer). The confining top layer of clay and peat is on average 4 m thick. The upper aquifer of Holocene and Pleistocene sands has a thickness of 20 to 60 m and is divided from the lower aquifer by a 5 m thick clayey aquitard that is sometimes absent. The geohydrological base varies from a depth of 130 m in the northern part to 30 m in the southern part of the study area. For the development of rainwater lenses in saline groundwater, the shallow part of the geohydrology of the study area, i.e. the upper aquifer and confining top layer, is of main interest.

3 Materials and methods

3.1 Mapping rainwater lenses

We used different geophysical and hydrological techniques to map the characteristics of rainwater lenses on top of upward-seeping saline groundwater. We carried out the measurements at different spatial scales, varying from field to island scale. As salinity changes rapidly in space and with depth, we needed high-resolution techniques that could record this variability. We applied the following in situ techniques to obtain detailed salinity-depth profiles: electrical soil conductivity measurements using the TEC-probe, groundwater sampling at small depth intervals, and electrical cone penetration tests (ECPT). We used ex situ continuous vertical electrical soundings (CVES) and surface electromagnetic measurements (EM31) to map the spatial variation of rainwater lenses within an agricultural field (0.05 km^2). A helicopter-borne frequency-domain electromagnetic (HEM) survey was performed to map the thickness of rainwater lenses for a large area on the island of Schouwen-Duivenland (56 km^2). Figure 4a–d shows the locations of the different measurements in the study area. At site 11 (Fig. 4c), we applied all our measurement techniques to compare their results and to improve the inversion models of the geophysical techniques. This site was chosen because of its position at a transition from a low-lying, clayey reclaimed salt marsh at −0.7 m m.s.l. to a higher sandy creek ridge lying at −0.2 m m.s.l. (Fig. 4c). The measurement techniques will be described briefly below.

HESSD
8, 7657–7707, 2011

3.1.1 TEC-probe

The TEC-probe is suitable for manual 1-D in situ measurements of temperature and the apparent electrical conductivity (EC_a) of soft soils like peat and clayey soils (Van Wirdum, 1991). We carried out TEC-probe measurements at 27 agricultural sites with differing geohydrology and geomorphology (Fig. 4a). At each site, TEC-probe measurements were done in a ditch and at different distances from the ditch, from the groundwater level downward at 0.1 m intervals until a depth of 4.0 m. Measured EC_as were automatically corrected to obtain a specific EC_a for a reference temperature of 25 °C. To obtain the electrical conductivity of groundwater (EC_w), EC_a must be multiplied by the formation factor (FF), which depends mainly on the lithology (Archie, 1942; Keary and Brooks, 1991; Friedman, 2005). We determined the formation factor (FF) for seven different soil types based on 584 measured EC_w – EC_a pairs (Table 1). EC_a was measured with the TEC-probe and EC_w was obtained by groundwater sampling. EC_w-values were transformed to chloride concentrations using a calibration curve based on a linear regression analysis ($R^2 = 0.98$) of 79 groundwater samples: Cl ($\mathrm{g\,l^{-1}}$) $= EC_w$ ($\mathrm{mS\,cm^{-1}}$)$\cdot$0.36–0.45. Simultaneously with the TEC-probe measurement, we made a detailed soil description to assess the formation factor.

3.1.2 Groundwater sampling

From the 27 TEC-probe sites we selected two sites on the island of Schouwen-Duivenland, site 11 (Fig. 4c) and site 26 (Fig. 4d), where we installed clusters of piezometers for sampling groundwater to derive chloride-depth profiles. The clusters were installed in ditches and at different distances from the ditches in the fields (Fig. 4c–d). The clusters in the fields were located between two drains, except for the two clusters mp 5 and mp 6 (mp = monitoring point) at site 26. These two clusters were positioned near (<0.2 m) a drain to measure the effect of tile drainage. Each cluster contained 6 to 7 piezometers with 0.16 m long screens at depths of 0.8 m, 1.0 m, 1.3 m, 1.6 m, 2.0 m, 3.0 m and 4.0 m below ground level (b.g.l). Before taking groundwater

HESSD
8, 7657–7707, 2011

Shallow rainwater lenses in deltaic areas with saline seepage

P. G. B. de Louw et al.

samples, we extracted all the water from the piezometers and waited several hours until the piezometers had re-filled with groundwater. The electrical conductivity of the sampled groundwater was measured in the field and chloride was analyzed in the laboratory. Hydraulic heads were measured as well to determine the head change with depth. Heads were corrected for density differences by conversion to fresh water heads (Post et al., 2007).

3.1.3 Continuous vertical electrical soundings: CVES

We carried out the CVES-measurements in profiles (with a length of 150 to 350 m) perpendicular to the ditches at 8 of the 27 TEC-probe sites (Fig. 4a). Some of the results and a detailed set up of the CVES-measurements were described in Goes et al. (2009). The CVES measurements were done with an AbemSAS4000 connected to four multi-electrode cables, with electrode spacing of 1 m to obtain a detailed resolution both horizontally and in depth. The measured electrical resistivity data were inverted into real soil resistivities using SensInv2-D (Geotomographie, 2004).

3.1.4 Electromagnetic EM31 survey

We carried out an EM31-survey at site 11 to obtain an overview of the spatial variation of groundwater salinity in the shallow subsoil within one agricultural field. The EM31 is an electromagnetic instrument that measures the average apparent electrical conductivity of the shallow subsoil (McNeill, 1980). The average penetration depth of these measurements was about 6 m, which is less than the penetration depth of the CVES-measurements (about 20 m). However, the EM31-measurements allowed us to map a larger area in a horizontal plane (about 0.1 km^2). The EM31-measurements with a spacing of 5 m have been interpolated to a conductivity map, which represents the bulk conductivity of the top 6 m of the subsoil.

HESSD
8, 7657–7707, 2011

3.1.5 Helicopter-borne electromagnetic measurements (HEM)

A helicopter-borne survey was conducted by the airborne geophysics group of the German Federal Institute for Geosciences and Natural Resources (BGR) in August 2009 (Siemon et al., 2011). The survey, covering a large part of the island of Schouwen-Duivenland (Fig. 4b), was flown within two days. Three survey flights were needed to map an area of about 56 km^2 with 31 WNW-ESE lines and 16 NNE-SSW tie lines at 200 m and 500 m line spacing, respectively, totalling 313 line-km. Electromagnetic, magnetic and radiometric data, as well as position data, were acquired simultaneously. The electromagnetic system we used was a RESOLVE towed "bird" consisting of five horizontal-coplanar (HCP) coil systems and one vertical-coaxial (VCX) coil system, with measuring frequencies ranging from 387 Hz to 133 kHz. The average sensor altitude was 33 m above ground level. About 84 300 1-D resistivity-depth inversion models were derived from the HCP data using a single-site Marquardt-Levenberg inversion procedure for the few-layers as well as for the smooth multi-layer inversion approach (Siemon et al., 2009).

3.1.6 Electrical cone penetration tests (ECPT)

We contracted a geotechnical company (www.bmned.com) to carry out 23 ECPTs on Schouwen-Duivenland to obtain 1-D in situ salinity profiles down to a depth of 25 m (Fig. 4b). The technique is comparable with a manual TEC-probe measurement but can also be applied in sandy soils and down to greater depths. Besides measurements of the soil's apparent electrical conductivity (EC_a) during penetration, the cone sleeve and tip friction were also measured to determine the lithological composition (BMNED, 2011). The ECPTs were carried out in the HEM pilot area (Fig. 4b) in order to derive conductivity depth profiles, which could be subsequently used to check the calibration of the HEM system and to optimize the inversion of the HEM data.

HESSD
8, 7657–7707, 2011

3.2 Numerical modelling of rainwater lenses

We constructed two different types of groundwater models to increase our insight into rainwater lenses on top of saline groundwater: (1) a 3-D-model that was able to reproduce the field measurements to ensure that we had incorporated the most important parameters, and (2) various smaller-scale 2-D conceptual models to focus on the mixing of saline seepage and infiltrating rainwater, and the flow to drains in detail. These models were used to analyse the sensitivity of different parameters.

3.2.1 Set-up of 3-D-model

We set up the 3-D-model with the numerical transport code MOCDENS3-D (Oude Essink, 2001a; Oude Essink et al., 2010) for a small area (1 km^2) at a transition from a low-lying, clayey reclaimed salt marsh to a higher sandy creek ridge (site 11, Fig. 4b–c). Different kinds of measurements were available for this site to evaluate the performance of the model. The model area was divided into cells of 5 by 5 m and the subsoil was divided into 41 layers of 0.3 to 5 m, up to a maximum depth of 35 m, to accurately model the local fresh-saline processes. The geohydrological schematization and parameterization was based on our field measurements and the Dutch Geohydrological Information System (REGIS II, 2005). The molecular diffusion coefficient D_m for porous media was assumed to be $8.6 \times 10^{-5}\ m^2\ d^{-1}$. The longitudinal dispersivity was set equal to 0.1 m and the ratio transversal to longitudinal dispersivity was 0.1. These rather small values are based on numerous case studies of Dutch and Belgian aquifer systems with marine and fluvial deposits (e.g. Stuyfzand, 1993; Lebbe, 1999; Oude Essink, 2001b; Vandenbohede and Lebbe, 2007). Fixed heads were applied at the model boundaries and were deduced from the regional groundwater model of the province of Zeeland (Van Baaren et al., 2011). The period of 1906–2006 was simulated with stress periods of 10 days. Recharge was calculated from precipitation and evapotranspiration data from two nearby meteorological stations (Kerkwerve and Wilhelminadorp) of the Royal Netherlands Meteorological Institute (KNMI). A 100-yr simulation period was

HESSD
8, 7657–7707, 2011

long enough for the groundwater chloride distribution at the sandy creek ridges to reach a state of equilibrium with the boundary conditions.

3.2.2 Set-up of 2-D-model

From the 3-D-model we zoomed into low-lying seepage areas to focus on the mixing of infiltrating fresh rainwater and upward-seeping saline groundwater between two ditches. Based on our findings with the 3-D-model and our field measurements, we constructed a conceptual cross-sectional 2-D-model between two ditches of a tile-drained agricultural field with upward-seeping saline groundwater (Fig. 5). For this modelling exercise we used the numerical transport code Seawat (Langevin et al., 2003). The cell size in a horizontal direction was 1 by 1 m and the layer thickness in the vertical direction was 0.1 m. The total thickness of the reference model was 3.0 m, which equals the thickness of the confining layer. Parameter values for the reference model and sensitivity models are given in Table 2 and are based on field data and the 3-D-model. For seepage areas our measurements show a permanently higher hydraulic head in the upper aquifer than in the confining layer. Moreover, the head difference was relatively constant throughout the year. We therefore assumed a permanent upward groundwater flow from the upper aquifer into the Holocene confining layer, with a constant flux Q_s and chloride concentration $\mathrm{Cl_s}$ throughout the year (Fig. 5). Although the confining layer consists of a sequence of different soil types, we considered it to be homogeneous. The effect of soil composition heterogeneity is addressed in the sensitivity analysis by applying a very low permeable layer at different depths in the confining layer, as we think this may influence groundwater flow and solute transport in the shallow groundwater system.

The initial groundwater chloride concentration in all model layers was set equal to the chloride concentration of the upward-seeping groundwater $\mathrm{Cl_s}$. A rainwater lens can develop in this saline groundwater body under a varying recharge of fresh rainwater ($\mathrm{Cl} = 0.02\,\mathrm{g\,l^{-1}}$). Daily values of recharge were determined from daily precipitation P and potential reference crop evapotranspiration ET at the nearby weather stations. We

HESSD
8, 7657–7707, 2011

used data from the year 2005 because these were representative for the annual precipitation surplus, and applied them for every year during the whole simulation period. A simulation period of 30 yr was long enough for all model simulations to reach a stationary situation, which means that the annual mass balance did not change significantly from year to year. The model output was analysed for year 30.

3.2.3 Sensitivity analysis

We carried out a sensitivity analysis with the 2-D-model for 19 model parameters, which are mainly physical and geographical parameters (Table 2). One parameter at a time was modified while the others remained fixed. The modified parameter values were based on field measurements and surveys, and geographical and geological data; they represent plausible ranges for the study area. We tested the parameter sensitivity for rainwater lens characteristics for a location in the middle between two drains (bdr) and for a location at a drain (dr), both at the largest possible distance from the ditches (Fig. 5). Besides the sensitivity analysis, we used results from the 2-D-models to study vertical flow processes in more detail at and between the drains with respect to lens characteristics.

4 Results and discussion

4.1 Characteristics of the mixing zone in seepage areas

The precise form of the mixing zone between infiltrating rainwater and saline groundwater was obtained accurately with the 1-D in situ measurements by the TEC-probe (Fig. 6) and ECPT soundings (Fig. 7). At 17 of the 27 TEC-probe sites, we measured a clearly S-shaped mixing zone between rainwater and saline groundwater; these are shown in Fig. 6. At the other 10 locations, we found a constant and fresh groundwater profile with depth. The measured S-shaped mixing zones are well described by the spatial moment method (Eeman et al., 2011). With this method the chloride concentration change with depth, i.e. the derivative of the chloride profile, is described by a normal distribution function, from which the centre of mass (1st moment) indicates the centre of the mixing zone D_{mix} (Fig. 6). The variance (2nd moment) is a measure of the extent of the mixing zone. By fitting the normal distribution function through the measurements, we derived five characteristics from it (Fig. 6): the depth of the centre of the mixing zone D_{mix}, the bottom of the mixing zone B_{mix}, the half-width of the mixing zone $W_{mix}(= D_{mix} - B_{mix})$, and the minimum and maximum chloride concentrations Cl_{min} and Cl_{max}. B_{mix} was defined as the depth where the chloride concentration was 99 % of Cl_{max}. We used these lens characteristics in the further analysis of our measurements and model results.

The lens characteristics D_{mix}, B_{mix} and W_{mix} derived from the TEC-probe and ECPT measurements are summarized in Table 3. In the seepage areas, the depth of the centre of the mixing zone was found to be very shallow with a median depth of D_{mix} of 1.7 m b.g.l. Mixing occurred no deeper than 5.5 m depth (= B_{mix}) and always in the confining layer. TEC-probe results showed a large variation of Cl_{max}, 0.9 g l^{-1} to 15.7 g l^{-1} (Fig. 6). The ECPT salinity profiles, which go much deeper than TEC-probe profiles, showed that below the mixing zone the salinity remains relatively constant (at value Cl_{max}) until a depth of at least 25 m (Fig. 7). However, there was one exception: ECPT-12 was located in a seepage area at about −1.5 m b. m.s.l. and showed a constant fresh water profile to a depth of 25 m. The contrast with the salinity profile of ECPT-13 (D_{mix} at 1.5 m below ground level), which lies only 600 m from ECPT-12 and at the same elevation is large. However, the explanation was rather simple: the fresh water profile at ECPT-12 was caused by lateral fresh groundwater flow from the elevated dunes (at 1 km to the west) that does not reach ECPT-13. The ECPTs are additionally valuable for the thicker rainwater lenses in the elevated areas, such as the sandy creek ridges (e.g. ECPT-32 and ECPT-4 in Fig. 7). Nine ECPTs were made at the sandy creek ridges where D_{mix} varied between 4 and 11 m depth, and B_{mix} varied between 8 and 14 m depth (Table 3).

HESSD
8, 7657–7707, 2011

The TEC-probe and ECPT data showed there was no sharp boundary between infiltrating fresh rainwater and saline seepage groundwater, but a gradual mixing zone with a median half-width W_{mix} of 0.9 m. Although this is much smaller than at the sandy creek ridges with a median W_{mix} of 3.0 m (Table 3) and what is usually found for BGH-lenses on islands and dunes (e.g. Fetter, 1972; Underwood et al., 1992; Stuyfzand, 1993; Sakr, 1999), the mixing zone in the seepage areas can be labelled as relatively wide compared to its depth. Therefore, the analytical and numerical approaches that assume a sharp interface and satisfactorily simulate BGH-lenses (e.g. according to Van der Veer, 1977; Van Dam and Sikkema, 1982; Sikkema and Van Dam, 1982; Sakr, 1999; Boekelman, 2001) should not be applied to these shallow rainwater lenses. As the mixing zones manifest at shallow depth, their position and width is of great importance for the fresh water available for crop growth. In most seepage areas, we did not find any fresh groundwater (i.e. Cl-<0.3 g l^{-1}). The upper groundwater is already a mix of seepage water and rainwater, which indicates that part of the mixing process very likely occurs in the unsaturated zone.

4.2 Rainwater lens variation within agricultural fields

4.2.1 Monitoring results at agricultural sites 11 and 26

Figure 8 shows the chloride-depth profiles derived from groundwater samples at different locations within the agricultural fields of site 11 and site 26 (for location, see Fig. 4c–d). For both sites, we measured a relatively constant chloride depth profile beneath the ditch, with a chloride concentration of 16 g l^{-1} for site 11 and 12 g l^{-1} for site 26. In contrast to the locations in the field, there was no mixing beneath the ditch and upward flowing saline groundwater exfiltrates in the ditches without mixing. At most monitoring locations in both fields, the same salinities as beneath the ditches were found at 3 to 4 m depth, but upwards from here the salinity decreased, indicating the presence of the mixing zone. Although there were no significant differences in mixing zone characteristics for the different distances from the ditch at site 26, the position in

HESSD
8, 7657–7707, 2011

relation to the drains did have an impact on the mixing zone. The monitoring locations near drains showed a smaller mixing zone at a shallower depth when compared to the monitoring locations between drains (site 26, Fig. 8).

In agricultural site 11 we found a large spatial variation in the salinity profiles (Fig. 8). Within about 200 m, the salinity at 2 to 4 m depth increased from fresh (Cl = 0.03–0.05 g l^{-1}) at the sandy creek ridge, mp 10, to almost seawater (Cl = 14 to 16 g l^{-1}) in the lower-lying clay area, mp 1 to mp 7. Location mp 8 showed an intermediate salinity profile between these two extremes (Fig. 8). This large spatial salinity gradient at site 11 was identified by all the measuring techniques we used (i.e. groundwater sampling, TEC-probe, ECPT, CVES, EM31, HEM). D_{mix} and B_{mix} derived from TEC-probe and ECPT measurements were plotted in a cross-section as well as the measured fresh water heads at 1.5 m and 4 m depth (Fig. 9). Although the spatial variation of rainwater lens thickness could be followed nicely with the CVES-measurement, the exact lens characteristics D_{mix} and B_{mix} could not be derived. This is due to the fact that the penetration depth could not be derived exactly from the electrical measurements. As such, we plotted the 3 Ωm isoline of the real inverted soil resistivity in the cross-section to illustrate the strong gradient in salinity profiles (Fig. 9).

As the confining layer was about 2.5 to 3 m thick at site 11, the fresh water head at 4 m depth represents the regional hydraulic head of the upper aquifer. In the seepage area, where D_{mix} is shallower than 2 m, the fresh water head at 4 m depth is permanently higher than the fresh water head at 1.5 m depth (Fig. 9). The average fresh water head difference is about 0.1 m (mp 5 to mp 8) increasing towards the NW-ditch with a maximum fresh water head difference in the ditch of 0.65 m. This large fresh water head difference at the ditch hinders the infiltration of surface water and results in a constant salinity profile ($D_{mix} = B_{mix}$). At the elevated sandy creek ridge, the fresh water head at 4 m depth is about 0.1 m lower than at 1.5 m depth, creating a downward flow and a much thicker rainwater lens with D_{mix} at 4 to 7 m depth and B_{mix} at 8 to 10 m depth. The strong upconing of saline groundwater was remarkable at the SE-ditch in the sandy creek ridge at only a few metres distance from the area where rainwater

HESSD
8, 7657–7707, 2011

infiltrates to a large depth (Fig. 9). Due to the low surface water level maintained in the ditch of −1.95 m m.s.l. (the same as for NW-ditch), the approximately 0.6 m higher fresh water head in the upper aquifer creates a strong upward flow of saline groundwater. The fresh water head and salinity measurements at site 11 prove that the vertical flux direction (seepage or infiltration) with small fresh water head differences can cause large differences in rainwater lens thickness.

4.2.2 Comparison of 3-D-model and monitoring results at site 11

The techniques applied at agricultural site 11 are complementary to each other, varying from 1-D in situ absolute chloride profiles (down to 4 m depth) and 1-D in situ ECPT salinity profiles (down to 25 m depth) to the 2-D and 3-D surface measurements (CVES, EM31 and HEM) to follow the spatial variation of the rainwater lenses. This made the site suitable for testing the numerical concepts and parameters to simulate rainwater lenses in saline groundwater in both an infiltration and a seepage situation. Figure 10 shows the comparisons between the field observations and the model results for the 3-D-numerical model. We found that the spatial variation of the average, modelled, chloride concentration of the top 6 m (Fig. 10a) showed good agreement with the EM31-measurements (Fig. 10b): with low salinities on the sandy creek ridge and high salinities in the seepage area. The calculated bottom of the mixing zone (B_{mix}) at the sandy creek ridge was about 8 m below ground level, which is in agreement with the ECPT and HEM results (ECPT 32 in Figs. 7 and 11). The lateral variation of rainwater lens thickness measured by the 1-D in situ techniques (D_{mix} and B_{mix}, see Fig. 9) and CVES (see Fig. 9 and Fig. 10e) is well reproduced by the numerical model (Fig. 10d). The measured chloride profiles, both absolute concentrations and the position and width of the mixing zone, showed good agreement with the modelled profiles (Fig. 10c). To summarize, the current fresh and saline groundwater system could be simulated well with the 3-D numerical model.

4.2.3 Results of 2-D-model

The findings of the 3-D-model (parameterization and schematization) were used to construct the conceptual 2-D-model for the seepage area. Figure 12 shows the results of the 2-D reference model. Upconing of saline groundwater at the drains was clearly visible, whereas the rainwater lens reached a greater depth between the drains (Fig. 12a and b). This corresponds with the measurements at site 26 (Fig. 8). The chloride profile and fresh water head were plotted for a location between two drains, and at a drain (Fig. 12b–c). This was done for the time step with the highest fresh water heads (wet period) and for one with the smallest fresh water heads (dry period). The heads between the drains are significantly higher than at the drains for the wet period. In the dry period, when heads dropped below drain level, the heads were equal. The large difference between the wet and the dry period for the heads is in contrast with the chloride profiles, which only showed little temporal variation. This will be discussed in Sect. 4.4.

The sensitivity of 19 model input parameters was tested for the lens characteristics; the centre depth D_{mix}, the bottom B_{mix} and the half-width W_{mix} of the mixing zone. Figure 13 shows the results for the model parameters with an effect larger than 0.1 m on one of these lens characteristics compared with the reference model. As D_{mix}, B_{mix} and W_{mix} did not fluctuate much through the whole period (yearly amplitude about 0.1 m), we presented average values in Fig. 13. The effects on D_{mix} and B_{mix} were more evident between the drains than at the drains. The parameters for seepage flux Q_{s}, precipitation surplus P-ET and drainage depth h_{dr} had the largest effect on D_{mix} and B_{mix}. Larger Q_{s} and smaller P-ET led to a mixing zone at shallower depth. D_{mix} at the drains was always within 0.1 m of the applied drainage depth h_{dr}. The longitudinal dispersivity α_l was obviously the principal factor for W_{mix}. The other parameters not presented in Fig. 13 (including the chloride concentration of the seepage $\mathrm{Cl_s}$, drainage resistance of the drains Ω_{dr}, drainage resistance of the ditch bottom Ω_{ditch}, and porosity n) did not significantly influence the lens. The results of the sensitivity analysis will be further discussed in Sects. 4.5, 4.6 and 4.7.

Discussion Paper | Discussion Paper | Discussion Paper | Discussion Paper |
HESSD
8, 7657–7707, 2011

4.3 Spatial variation of rainwater lens thickness: HEM results

The HEM data inverted to layered-earth resistivity-depth models reveal the spatial distribution of the electrical conductivity down to depths of about 20–30 m in the lowlands and of more than 60 m in the dune area. Conductivity contrast of fresh and saline groundwater dominates the inverted HEM models rather than differences in lithology. 2-D cross-sections were produced for all survey lines. As an example, part of WNW-ESE line 9 is shown in Fig. 11 crossing the agricultural field of site 11 and the sandy creek ridge. The results of the smooth multi-layer HEM models agree very well with nearby ECPT measurements, which are plotted as coloured columns in the cross-section. Only ECPTs having a horizontal distance of less than the footprint size of the HEM measurements (about 150 m) were projected to the flight-line. Figure 7 shows a comparison of six ECPT soundings and corresponding HEM models at site 11 (ECPT 31, 2, 32, 4) and close to the dune area (ECPT 12 and 13).

The analysis of the mixing zone derived from the detailed TEC-probe and ECPT data showed that the depth of the centre of the mixing zone, D_{mix}, is a consistent and easy to determine parameter to characterize the rainwater lens. We used D_{mix} to indicate the thickness of the rainwater lens. To derive D_{mix} from the HEM data, we determined the depth of the strongest vertical conductivity gradient according to the spatial moment method described in Sect. 4.1. Below this strongest gradient, the resistivities are mostly less than 3 Ωm (EC < 3.3 mS cm^{-1}). This was done for the 84 300 1-D resistivity-depth inversion models and interpolated to a 50 m grid size map (Fig. 14) representing D_{mix} for the entire airborne survey area. In a large part of the survey area (>50 %) the mapped rainwater lens was thinner than 2 m. Thicker rain water lenses occurred in the eastern part of the survey area (D_{mix} = 5–10 m b.g.l.), close to agricultural field 11 and the adjacent fossil sandy creek (D_{mix} = 8–20 m b.g.l.) and, of course, in the dune area (D_{mix} > 20 m b.g.l.).

HESSD
8, 7657–7707, 2011

The HEM-survey on the island of Schouwen-Duivenland made it possible to analyse the spatial variation of rainwater lenses by correlating D_{mix} derived from the 84 300 HEM-measurements, to geographically varying features. The thickness of the rainwater lens, D_{mix}, was clearly related to surface elevation (Fig. 15a) and to seepage and infiltration fluxes (Fig. 15b). Hence surface elevation and seepage/infiltration flux were strongly correlated; seepage occurred in low-lying polders below sea level and infiltration occurred in dunes, sandy creek ridges and agricultural areas above sea level (compare Fig. 2c with 2e). The measurements showed that rainwater lenses in low-lying seepage areas were, on average, 2 m thick (i.e. from ground level to D_{mix}). The thinnest rainwater lenses were found in areas below −2 m m.s.l. There was a sharp increase in thickness when vertical flow changed from seepage to infiltration (Fig. 15b). This shows that vertical flow (seepage or infiltration and fluxes) is the mechanism that controls the development of rainwater lenses.

4.4 Vertical flow tipping point

Both the fresh water head and salinity measurements at site 11 (Fig. 9) and the correlation of D_{mix} with seepage/infiltration flux (Fig. 15) show that rainwater lens thickness is mainly the result of the vertical head gradient and vertical flow. To extend the understanding of the role of vertical flow on rainwater lens characteristics, we studied the vertical head and flux profiles of the 2-D-model results in more detail. Here we introduce the vertical flow tipping point (FLTP), which is the depth below ground level where the downward flow component meets the upward flow component. This point is best illustrated with a fresh water head depth profile at a drain, see Fig. 12c. Drainage of groundwater causes a dip of the hydraulic head at the drains, which results in groundwater flow towards the drain from both above and below. As variable density flow is driven by both head gradients (forced convection) and density differences (free convection), we determined FLTP from the calculated vertical fluxes directly rather than deriving it from the calculated fresh water head gradients. Figure 12d shows the daily FLTP for a period of 1 yr for the reference model. At the drains, the FLTP is always at drainage level, except in the periods when groundwater levels drop below the drains.

HESSD
8, 7657–7707, 2011

Then the vertical flow component is upwards for the entire saturated profile and the FLTP equals the groundwater level. The FLTP between the drains is much more variable with time than the FLTP at the drains. The maximum depth of FLTP between the drains was 2.35 m, which occurred when the groundwater level was at its maximum and causing the largest downward head gradient. When the groundwater level dropped, the FLTP moved to shallower depth and upward flow became more important. During the dry season, when groundwater levels dropped below the drains, there was only upward groundwater flow and the FLTP was equal to the groundwater level. The temporal variation of FLTP was driven by groundwater level fluctuations resulting from the daily variation of precipitation and evapotranspiration.

The FLTP time series were determined for all 76 sensitivity models, for which the parameters are listed in Table 2, as well as the correlation with the lens characteristics D_{mix}, B_{mix} and W_{mix}. For nearly all sensitivity cases, the FLTP at the drains was situated at drainage level during periods when groundwater levels were above drainage level. The depth of the centre of the mixing zone, $D_{\text{mix},}$, at the drain was also situated at drainage level in 90 % of the sensitivity cases. The calculated (Fig. 12a) and measured (Fig. 8) upconing of saline groundwater at the drains confirmed the large impact of drains on the rainwater lenses. Although D_{mix} was fixed at the drains, D_{mix} between the drains was much more variable between the different sensitivity cases (see Fig. 13) and other parameters played an important role. For every sensitivity model, the average FLTP was determined from the FLTP-time series and plotted against D_{mix} (Fig. 16). The scatter plot shows that D_{mix} between the drains had a strong linear and positive correlation with the average FLTP between the drains ($R^2 = 0.91$). Thus we have established that the vertical flow direction within the confining layer plays a major role in determining the depth of the centre of the mixing zone.

It is remarkable that the large variation of FLTP between the drains during the year resulted in a fairly steady depth of the mixing zone (maximum yearly amplitude = 0.1 m). This can be explained by the fact that flow velocities were very small compared to the daily change of the FLTP. The calculated average flow velocity of the downward flow

HESSD
8, 7657–7707, 2011

component between the drains was 1.2 mm d^{-1}, with a maximum of 6 mm d^{-1} and the average flow velocity of the upward flow component is 0.5 mm d^{-1} with a maximum of 0.8 mm d^{-1}. The daily change of the FLTP causes water particles to move both up- and downwards. The upward or downward movement of a water particle is not exactly vertical because its flow path is the result of both the vertical and horizontal flow components. The calculated horizontal flow velocities were on average 1.7 times larger than the vertical flow velocities. The sequence of the changing vertical flow direction indicated by the FLTP and corresponding net flow velocity is the main mechanism of the mixing process between rainwater and saline seepage.

The bottom of the mixing zone B_{mix} between the drains corresponded approximately with the maximum depth of FLTP (Fig. 16). This was the maximum depth where downward flow occurred. The flow direction below FLTP-max is always upward so that no flow-driven mixing with groundwater occurs. Mixing below FLTP-max can therefore only result from molecular diffusion and is of minor importance compared to the flow-driven mixing. At the drains, B_{mix} was always below drainage depth and in most cases even 0.5 to 1.0 m deeper than FLTP-max at the drains. Additionally, B_{mix} at the drains was correlated with B_{mix} between the drains ($R^2 = 0.46$), which indicates that mixing below the drains occurred by upward flow of groundwater that was infiltrated between the drains.

4.5 Controlling factors: geohydrology, drainage, seepage flux and recharge

Our measurements show that the mixing of the upward flowing saline groundwater with infiltrating rainwater occurred in the confining top layer. This was caused by the permanently higher fresh water heads in the upper aquifer compared to the lower part of the confining top layer. FLTP-max was therefore always situated within the confining layer and consequently also B_{mix}. Given that lenses in seepage areas develop within the confining layer, the heterogeneity of the confining layer may have an additional effect on the lens characteristics. The sequence of confining sediments with different vertical hydraulic conductivities determines the fresh water head change with depth within the confining layer. When these fresh water head gradients are large enough, they influence the FLTPs and therefore D_{mix} and B_{mix}. The sensitivity analysis showed that a 0.2 m thick low permeable layer ($k_v = 10^{-3}$ m d^{-1}) within the confining layer ($k_v = 10^{-2}$ m d^{-1}) had a significant impact when it was put in the upper 2 m of the confining layer (Fig. 13i, parameter d_{lpl}). When the low permeable layer was situated above the drains, drainage of groundwater was much more difficult, resulting in higher groundwater levels, deeper FLTPs and thicker rainwater lenses between the drains. A low permeable layer situated below the drains hinders the further downward flow between the drains, resulting in shallower FLTPs and thinner rainwater lenses between the drains.

The large impact of drainage depth on D_{mix} and B_{mix} was shown by our field measurements (Fig. 8) and sensitivity analysis (Fig. 13d, h_{dr}) and has been discussed in the previous sections. Besides the drainage depth, the magnitude of incoming fluxes, both from above (recharge) and below (seepage), had a large impact on lens characteristics (Fig. 13a–b, Q_s and P-ET). More recharge led to higher groundwater levels and consequently to deeper FLTPs and therefore to thicker rainwater lenses. Thinner lenses are calculated with larger upward-seepage fluxes, which cause the FLTPs to move upwards. The dominant role of the incoming recharge and upward-seepage fluxes makes the shallow rainwater lenses very vulnerable to climate change and sea level rise. The Royal Netherlands Meteorological Institute (KNMI) formulated four different climate scenarios which are equally likely to occur (Van den Hurk et al., 2006). The W^+ climate scenario is the driest (2.5 % reduction of precipitation and 7.5 % increase of evapotranspiration) and has the largest expected sea level rise of 0.85 m by the year 2100. A sea level rise would cause an increase of the hydraulic head in the aquifers, which would result in an increase of seepage flux. Both sea level rise and a reduction of the precipitation surplus may lead to thinner rainwater lenses. Since drainage depth is another important factor that determines rainwater lens thickness, adapting the tile drainage systems may effectively reduce the negative consequences of climate change and sea level rise. Thus, a better understanding of rainwater lenses could lead to practical measures for maintaining agriculture water storage systems.

4.6 Forced convection versus free convection

The sensitivity analysis showed that the salinity of the upward-seeping groundwater does not have a significant influence on lens characteristics. Therefore we suggest that free convection by density differences is of minor importance and lens characteristics in the seepage areas are principally controlled by forced convection due to head gradients. Simmons (2005) stated that even small concentration differences may lead to density-driven flow gradients equal to typical field-scale hydraulic gradients. Whether density-driven or head-driven flow is the dominant process results from a complex interplay between fluid and soil properties, and the competing demands of both free and forced convection and dispersion. Our proposition that forced convection dominates the rainwater lens development on top of saline seepage is supported by our different observations. Firstly, in seepage areas the hydraulic head in the upper aquifer was permanently higher than heads in the confining layer. This prevented the water from infiltrating to depths below the bottom of the confining layer. Secondly, large head gradients typically developed in these shallow groundwater systems, strongly influenced by intensive drainage and daily changing recharge. And thirdly, besides these large head gradients, the temporal variation of the FLTP played an important role. For depths above B_{mix}, the vertical flow direction changed throughout the year. During downward flow, free convection strengthened the head-driven forced convection, working in the same direction, whereas during upward flow the free convection opposed the forced convection. The net effect of free convection was diminished by this constantly changing vertical flow direction.

In contrast to the quick response of the intensively drained groundwater systems, there are the much slower responding groundwater systems where BGH-lenses develop; these slower systems have large drainage distances and no upward flow of saline water due to elevation like the dunes. The precipitation surplus is not drained but fully used for the recharge of the groundwater system. Under a relatively constant recharge regime, a downward head gradient causes the downward flow of rainwater to

HESSD
8, 7657–7707, 2011

much greater depths. In homogeneous aquifers, the vertical downward flow is only limited by the buoyancy force of the surrounding saline groundwater. This free convection-dominated system builds up much larger lenses than the head-driven forced convection flow in the intensively drained seepage areas. This difference in the lens developing mechanisms explains the sudden increase in lens thickness shown in Fig. 15b when moving from a seepage situation to one of infiltration.

5 Conclusions

We have described the characteristics and spatial variability of shallow rainwater lenses in areas with saline seepage and the mechanisms controlling them. Our findings are based on different types of field measurements and detailed numerical groundwater models applied in the south-western delta of the Netherlands. By combining various techniques, we were able to extrapolate the detailed in situ measurements at point scale (groundwater sampling, TEC-probe, ECPT) to field scale (CVES, EM31), and even to a larger area ($56\,km^2$) at regional scale using helicopter-borne electromagnetic measurements (HEM). We observed a gradual mixing zone between infiltrating fresh rainwater and upward-flowing saline groundwater. Below this mixing zone, the salinity stayed relatively constant with depth, with average chloride concentrations of 10 to $16\,g\,l^{-1}$. Point measurements by TEC-probe and ECPT-soundings were needed to determine the precise form of this mixing zone and to fully characterize the rainwater lenses. The mixing zone was S-shaped and best characterized by the depth of its centre D_{mix}, where the salinity was half that of seepage water, and by the bottom of the mixing zone B_{mix}, where the salinity was equal to that of the seepage water. Since salinity change with depth dominated the soil resistivity depth profiles obtained by TEC-probe and ECPT, the lens characteristics D_{mix} and B_{mix} could be determined without correcting for lithological formation and temperature. Additionally, D_{mix} was a consistent and easy-to-derive indicator for rainwater lens thickness and it can be mapped with HEM for large areas. However, groundwater sampling is always needed

HESSD
8, 7657–7707, 2011

to validate the geophysical measurements and to translate their soil resistivity values to groundwater salinity.

In the seepage areas, the centre of the mixing zone D_{mix} manifested at very shallow depth, on average 1.5 to 2 m below ground level, and the fresh water head in the upper aquifer was permanently higher than heads in the confining layer. This prevents the rainwater from infiltrating to depths below the bottom of the confining layer. In the higher lying infiltration areas, the vertical downward flow of rainwater was only limited by the buoyancy force of the surrounding saline groundwater. This led to much thicker rainwater lenses, varying from 5 to 15 m thick lenses in the sandy creek ridges to 100 m thick lenses in the dunes. Head-driven forced convection dominated the rainwater lens formation in the saline seepage areas rather than free convection due to density differences. Large head gradients developed in the confining layer due to drainage and the constantly changing recharge. The sequence of alternating vertical flow direction at low velocities caused by these head gradients plays a major role in determining the position of the mixing zone in seepage areas and in the mixing between rainwater and saline seepage. The vertical flow tipping point (FLTP), which is the depth below ground level where the downward flow component meets the upward flow component, was a valuable property for describing rainwater lens formation. Between drains, the FLTP was highly variable with time due to groundwater level fluctuations, whereas the FLTP at the drains was fixed at drainage level for most of the time. Despite the large temporal variation of the FLTP between the drains, the position of the centre of the mixing stays at a relatively constant depth (yearly amplitude was about 0.1 m) due to the alternating vertical flow directions at low velocities. The yearly average FLTP depth was linear and positively correlated with the position of the centre of the mixing zone D_{mix}. The maximum depth of the FLTP determined the bottom of the mixing zone B_{mix}. Between the drains, the yearly average FLTP and therefore average position of the mixing zone D_{mix} was mainly determined by the combination of seepage flux, recharge and drainage depth, whereas at the drains the controlling factor was drainage depth.

HESSD
8, 7657–7707, 2011

The dominant role of the incoming fluxes made the shallow rainwater lenses very vulnerable to climate change and sea level rise. Both sea level rise and a reduction of the precipitation surplus may lead to thinner rainwater lenses. Since drainage depth is another important factor that determines rainwater lens thickness, adapting the tile drainage systems may effectively reduce the negative consequences of climate change and sea level rise. Thus, a better understanding of rainwater lenses could lead to practical measures for maintaining agriculture water storage systems.

This study provides more information on the characteristics of shallow rainwater lenses and their spatial variation. Future work should be focussed on the temporal variations of the salinity of the upper part of the mixing zone and its interaction with soil moisture salinity in the root zone, especially since this can effect agriculture. As the mixing zones manifest at shallow depth, their position and width is of great importance for a sufficient supply of fresh water for crop growth. Capillary rise of saline groundwater may reach the root zone causing salt damage to crops. In most of these shallow rainwater lenses, we found no fresh groundwater, indicating that part of the mixing process very likely occurs in the unsaturated zone. As free convection by density difference did not significantly influence lens formation in areas with saline seepage, our findings on rainwater lens characteristics and formation mechanisms may also be applicable to wholly fresh groundwater systems. Rainwater lenses in brook valleys and wet meadows with groundwater discharge areas may limit the development of groundwater discharge-dependent ecosystems. The great advantage of studying rainwater lens formation in saline seepage areas arises from the large salinity contrast between rainwater and groundwater, which is easy to measure, even by non-invasive geophysical methods.

Acknowledgements. This research is part of CLIWAT, the Interreg IVb project (www.cliwat.eu), and of ‘Knowledge as an Asset’, the Deltares research programme. The work was carried out in collaboration with the province of Zeeland, the Scheldestromen Water Board and the Zuidelijke Land en Tuinbouw Organisation. We thank the following persons for helping collect the field data: Bart Goes, Tommasso Letterio, Francesco Sergi, Sjors Stevens, Bas De Veen, Corné Prevo, Valentina Marconi, Esther Vermue, Rien van den Hoek, and Jan van der Velde,

as well as the helicopter team of the German Federal Institute for Geosciences and Natural Resources (BGR), and particularly Angelika Ullmann for so thoroughly processing the HEM data.

References

Antonellini, M. and Mollema, P. N.: Impact of groundwater salinity on vegetation species richness in the coastal pine forests and wetlands of Ravenna, Italy, Ecol. Eng., 36(9), 1201–1211, 2009.

Archie, G. E.: The electrical resistivity log as an aid in determining some reservoir characteristics, Petroleum Transactions of AIME, 146, 54–62, 1942.

Badon Ghijben, W.: Nota in verband met de voorgenomen putboring nabij Amsterdam, Tijdschr, Van Koninklijk Instituut Van Ingenieurs, 5, 8–22, 1888 (in Dutch).

Bakker, M.: The size of the freshwater zone below an elongated island with infiltration, Water Resour. Res., 36(1), 109–117, 2000.

BMNED: Geotechnical research for CLIWAT pilot area B (climate change and water), Report 0100685/071032292, rev. B, 2011 (in Dutch).

Boekelman, R. H. Development of fresh water lenses. Proc. 16th Salt Water Intrusion Meeting, Miedzyzdroje, Wolin Island, Poland, 5–9, 2001.

Collins, W. H. and Easley, D.H.: Fresh-water lens formation in an unconfined barrier island aquifer, J. Am. Water Resour. Ass., 35, 1–22, 1999.

Custodio, E. and Bruggeman, G. A.: Groundwater Problems in Coastal Areas, Studies and Reports in Hydrology, UNESCO, International Hydrological Programme, Paris, 1987.

De Louw, P .G. B., Oude Essink, G. H. P., Stuyfzand, P. J., and Van der Zee, S. E. A. T. M.: Upward groundwater flow in boils as the dominant mechanism of salinization in deep polders, The Netherlands, J. Hydrol., 394, 494–506, 2010.

De Louw, P. G. B., van der Velde, Y., and van der Zee, S. E. A. T. M.: Quantifying water and salt fluxes in a lowland polder catchment dominated by boil seepage: a probabilistic end-member mixing approach, Hydrol. Earth Syst. Sci., 15, 2101–2117, doi:10.5194/hess-15-2101-2011, 2011.

Eeman, S., Leijnse, A., Raats, P. A. C., and Van der Zee, S. E. A. T. M.: Analysis of the thickness

HESSD

8, 7657–7707, 2011

Shallow rainwater lenses in deltaic areas with saline seepage

P. G. B. de Louw et al.

Title Page
Abstract Introduction
Conclusions References
Tables Figures
◄ ►
Back Close
Full Screen / Esc
Printer-friendly Version
Interactive Discussion

of a fresh water lens and of the transition zone between this lens and upwelling saline water, Adv. Water Res., 34(2), 191–302, 2011.
Fetter, C. W.: Position of the saline water interface beneath oceanic islands, Water Resour. Res., 8, 1307–1314, 1972.
Flowers, T. J.: Improving crop salt tolerance, J. Exp. Bot., 55, 307–319, 2004.
Friedman, P. S.: Soil properties influencing apparent electrical conductivity: a review, Computers and Electronics in Agriculture, 46, 45–70, 2005.
Geotomographie: SensInv2-D – Manual, available at: www.geotomographie.de, 2004.
Giambastiani, B. M. S., Antonellini, M., Oude Essink, G. H. P., and Stuurman, R. J.: Saltwater intrusion and water management in the unconfined coastal aquifer of Ravenna (Italy): a numerical model, J. Hydrol., 340(1–2), 91–104, 2007.
Goes, B. J. M., Oude Essink, G. H. P., Vernes, R. W., and Sergi, F.: Estimating the depth of fresh and brackish groundwater in a predominantly saline region using geophysical and hydrological methods, Zeeland, the Netherlands, Near Surface Geophysics, 7, 401–412, doi:10.3997/1873-0604.2009048, 2009.
Herzberg, A.: Die Wasserversorgung einiger Nordseebäder, J. Gasbeleucht. Wasserversorgung, 44, 815–819, 1901 (in German).
Jolly, I. D., McEwan, K. L., and Holland, K. L.: A review of groundwater–surface water interactions in arid/semi-arid wetlands and the consequences of salinity for wetland ecology, Ecohydrology, 1, 43–58, 2008.
Keary, P. and Brooks, M.: An Introduction to Geophysical Exploration, 2nd edition, Blackwell Science, 1991.
Katerji, N., Van Hoorn, J. W., Hamdy, A., and Mastrorilli, M.: Salinity effect on crop development and yield, analysis of salt tolerance according to several classification methods, Agr. Water Manag., 62(1), 37–66, 2003.
Langevin, C. D., Shoemaker, W. B., and Guo Weixing, W.: MODFLOW-2000, The US Geological survey Modular Ground-Water Model–Documentation of the SEAWAT-2000 Version with the Variable-Density Flow Process (VDF) and the Integrated MT3DMS Transport Process (IMT): US Geological Survey Open-file report 03-426, 2003.
Lebbe, L.: Parameter identification in fresh-saltwater flow based on borehole resistivities and freshwater head data, Adv. Water Resour., 22(8), 791–806, doi:10.1016/S0309-1708(98)00054-2, 1999.
Maas, K.: Influence of climate change and sea level rise on a Ghyben Herzberg lens, J. Hydrol.,

HESSD
8, 7657–7707, 2011

Shallow rainwater lenses in deltaic areas with saline seepage

P. G. B. de Louw et al.

347(2), 223–228, 2007.
McNeill, J. D.: Electromagnetic Terrain Conductivity at Low Induction Numbers. Geonics Ltd. Technical Note TN-6, Geonics Ltd., Mississauga, Ontario, Canada, 1980.
Meinardi, C. R.: Fresh and brackish groundwater under coastal areas and islands, GeoJournal, 7.5, 413–425, 1983.
Meisler, H., Leahy, P. P., and Knobel, L. L.: Effect of eustatic sea-level changes on saltwater-freshwater relations in the Northern Atlantic coastal plain, US Geological Survey Water-Supply Paper 2255, 1984.
Navoy, A. S.: Aquifer-estuary interaction and vulnerability of groundwater supplies to sea level rise-driven saltwater intrusion. Ph.D. thesis, Pennsylvania State University, USA, 1991.
Oude Essink, G. H. P.: Impact of sea level rise on groundwater flow regimes. A sensitivity analysis for the Netherlands. Ph.D. thesis Delft University of Technology, Delft Studies in Integrated Water Management, no. 7, ISBN 90-407-1330-8, 428 pp., 1996.
Oude Essink, G. H. P.: Salt water intrusion in a three-dimensional groundwater system in the Netherlands: a numerical study, Transport in Porous Media, 43(1), 137–158, 2001a.
Oude Essink, G. H. P.: Saltwater intrusion in 3-D large-scale aquifers: a Dutch case, Phys. Chem. Earth, 26(4), 337–344, 2001b.
Oude Essink, G. H. P., Baaren, E. S., and De Louw, P. G. B.: Effects of climate change on coastal groundwater systems: A modeling study in the Netherlands, Water Resour. Res., 46, W00F04, doi:10.1029/2009WR008719, 2010.
Post, V. E. A.: Groundwater Salinization Processes in the Coastal Area of The Netherlands due to Transgressions during the Holocene, Ph.D. thesis, Free University Amsterdam, 2004.
Post, V. E. A. and Abarca, E.: Saltwater and freshwater interactions in coastal aquifers, Hydrogeology J., 18(1), 1–4, 2010.
Post, V. E. A., Kooi, H., and Simmons, C.: Using hydraulic head measurements in variable-density ground water flow analyses, Ground Water, 45(6), 664–671, 2007.
REGIS II: Hydrogeological model of The Netherlands, Report: Vernes, R. W. and Van Doorn, Th. H. M., from Guide layer to Hydrogeological Unit, Explanation of the construction of the data set, TNO report NITG 05-038-B, available at: www.dinoloket.nl, 2005 (in Dutch).
Rozema, J. and Flowers, T.: Crops for a salinized world, Science, 322, 1578–1582, 2008.
Schot, P. P., Dekker, S. C., and Poot, A.: The dynamic form of rainwater lenses in drained fens, J. Hydrol., 293, 74–84, 2004.
Sakr, S. A.: Validity of a sharp-interface model in a confined coastal aquifer, Hydrogeology J.,

7(2), 155–160, 1999.
Siemon, B., Christiansen, A. V., and Auken, E.: A review of helicopter-borne electromagnetic methods for groundwater exploration, Near Surface Geophysics, 7, 629–646, 2009.
Siemon, B., Ullmann, A., Mitreiter, I., Ibs-von Seht, M., Voß, W., and Pielawa, J.: Airborne geophysical investigation of CLIWAT pilot areas, survey area Schouwen, The Netherlands, 2009, Technical Report, Interreg IVB Project: CLIWAT – Adaptive and sustainable water management and protection of society and nature in an extreme climate, BGR Archives-No. 0129932, Hanover, 2011.
Sikkema, P. C. and van Dam, J. C.: Analytical formulae for the shape of the interface in a semi-confined aquifer, J. Hydrol., 56, 201–220, 1982.
Simmons, C. T.: Variable density groundwater flow: From current challenges to future possibilities, Hydrogeology J., 13, 116–19, 2005.
Stafleu, J., Maljers, D. M., Gunnink, J. L., Menkovic, A., and Busschers, F. S.: 3-D modelling of the shallow subsurface of Zeeland, the Netherlands, Netherlands Journal of Geosciences, submitted, 2011.
Steppuhn, H. Van Genuchten, M. T., and Grieve, C. M.: Root-zone salinity. I. Selecting a product-yield index and response function for crop tolerance, Crop Science, 45(1), 209–220, 2005.
Stuyfzand, P. J.: Hydrochemistry and Hydrology of the Coastal Dune Area of the Western Netherlands, Ph.D. thesis, Free University Amsterdam, ISBN 90-74741-01-0, 366 pp., 1993.
Stuyfzand, P. J. and Stuurman, R. J.: Recognition and genesis of various brackish to hypersaline groundwaters in The Netherlands, in: Proc. 13th Salt Water Intrusion Meeting, edited by: Barrocu, G., University of Cagliari, Sardinia, 125–136, 1994.
Underwood, M. R., Peterson, F. L., and Voss, C. I.: Groundwater lens dynamics of atoll islands, Water Resour. Res., 28(11), 2889–2902, 1992.
Van Baaren, E. S., Oude Essink, G. H. P., Janssen, G. M. C. M., Louw, P .G. B. de, Heerdink, R., and Goes, B.: Freshening/salinization of phreatic groundwater in the province of Zeeland: Results of 3-D-density dependent groundwater model, Deltares Report, 2011 (in Dutch).
Van Dam, J. C. and Sikkema, P. C.: Approximate solution of the problem of the shape of the interface in a semi-confined aquifer, J. Hydrol., 56, 221–237, 1982.
Van den Hurk, B., Klein Tank, A., Lenderink, G., Ulden, A. van, Oldenborgh, G.J. van, Katsman, C, Brink, H. van den, Keller, F., Bessembinder, J., Burgers, G., Komen, G., Hazeleger, W., and Drijfhout, S.: KNMI Climate Change Scenarios 2006 for the Netherlands. KNMI, De Bilt,

Scientific Report WR 2006-01, 2006.
Van de Plassche, O.: Sea-level change and water-level movements in the Netherlands during the Holocene, Mededelingen Rijks Geologische Dienst, 36(1), 93 pp., 1982.
Van der Meij, J. L. and Minnema, B.: Modelling of the effect of a sea-level rise and land subsidence on the evolution of the groundwater density in the subsoil of the northern part of the Netherlands, J. Hydrol., 226(3–4), 152–166, 1999.
Van der Eertwegh, G. A. P. H., Nieber, J. L., De Louw, P. G. B., Van Hardeveld, H. A., and Bakkum, R.: Impacts of drainage activities for clay soils on hydrology and solute loads to surface water, Irrigation and Drainage, 55, 235–245, 2006.
Van de Ven, G. P. (Ed.): Man-Made Lowlands, History of Water Management and Land Reclamation in The Netherlands, Matrijs, Utrecht, 2003.
Van der Veer, P.: Analytical solution for steady interface flow in a coastal aquifer involving a phreatic surface with precipitation, J. Hydrol., 34, 1–11, 1977.
Van Rees Veilinga, E., Toussaint, C. G., and Wit, K. E.: Water Quality and hydrology in a coastal region of The Netherlands, J. Hydrol., 50, 105–0127, 1981.
Van Wirdum, G.: Vegetation and Hydrology of Floating Rich Fens, Ph.D. thesis, University of Amsterdam, 1991.
Vandenbohede, A. and Lebbe, L.: Effects of tides on a sloping shore: Groundwater dynamics and propagation of the tidal wave, Hydrogeol. J., 15(4), 645–658, doi:10.1007/s10040-006-0128-y, 2007.
Vandenbohede, A., Luyten, K., and Lebbe, L.: Impacts of global change on heterogeneous coastal aquifers: case study in Belgium, J. Coast. Res., 24(2B), 160–170, 2008.
Vos, P. and Zeiler, F.: Holocene transgressions of southwestern Netherlands, interaction between natural and antrophogenic processes, Grondboor & Hamer, 3–4, 2008 (in Dutch).
Voss, C. I. and Provost, A. M.: SUTRA, a model for saturated-unsaturated variable density groundwater flow with solute or energy transport, manual, US Geological Survey, Reston, Virginia, USA, 2008.
Weert, F. Van der Gun, J., and Reckman, J.: Global Overview of Saline Groundwater occurrence and Genesis, Report no. GP 2009-1, 2009.

HESSD
8, 7657–7707, 2011

Shallow rainwater lenses in deltaic areas with saline seepage

P. G. B. de Louw et al.

Table 1. Formation factors (FF) for different lithological units.

Lithology	Average FF	Std	No. of samples
Peat	2.1	0.7	41
Clay	2.5	0.6	192
Sandy clay/clayey sand	2.8	0.8	52
(Clayey) fine sand	3.2	0.4	299
Medium coarse sand	4*		
Coarse sand	5*		
Sand with gravel	6–7*		

* FF taken from Goes et al. (2009).

HESSD
8, 7657–7707, 2011

Table 2. Parameter values of 2-D reference model (Ref) and four sensitivity models (Ref−−, Ref−, Ref+, Ref++).

	Parameter	Description	Unit	Ref −−	Ref−	**Ref**	Ref+	Ref++
1	Q_s	seepage flux	$mm\,d^{-1}$	0.05	0.15	**0.25**	0.5	1.0
2	P-ET	recharge (average)	$mm\,d^{-1}$	0.25	0.5	**0.75**	1.0	1.25
3	Cl_s	Cl-conc seepage	$g\,l^{-1}$	0.15	5.0	**10.0**	15.0	19.0
4	L_{dr}	spacing between 2 subs. drains	m	2.5	5	**10**	15	20
5	h_{dr}	depth of drains	m	−1.4	−1.2	**−1**	−0.8	−0.6
6	Ω_{dr}	drainage resistance	d	0.5	1	**2.5**	5	7.5
7	L_{ditch}	spacing between 2 ditches	m	25	50	**100**	150	200
8	h_{ditch}	surface water level	m	−1.75	−1.5	**−1.25**	−1	−0.75
9	Ω_{ditch}	drainage resistance ditch	d	1	2.5	**5**	10	20
10	D_{conf}	thickness confining layer	m	0	2	**3**	4.5	6
11	k_v	vert. hydr. conductivity of confining layer	$m\,d^{-1}$	0.1×10^{-2}	0.5×10^{-2}	$\mathbf{1.0\times10^{-2}}$	2.5×10^{-2}	5.0×10^{-2}
12	k_h/k_v	anisotropy factor (k_v=constant)	–	1	2.5	**5**	7.5	10
13	n	porosity	–	0.06	0.1	**0.14**	0.18	0.22
14	γ_s	specific yield	–	0.15	0.2	**0.25**	0.3	0.35
15	d_{lpl}	depth low permeable layer (LPL)	m	−0.7	−1.0	**none**	−1.5	−2.5
16	$k_{v-lpl,1.5}$	k_v of LPL, depth LPL = −1.5 m	$m\,d^{-1}$	0.3×10^{-3}	0.6×10^{-3}	$\mathbf{1.2\times10^{-3}}$	2.4×10^{-3}	4.8×10^{-3}
17	$k_{v-lpl,2.5}$	k_v of LPL, depth LPL = −2.5 m	$m\,d^{-1}$	0.3×10^{-3}	0.6×10^{-3}	$\mathbf{1.2\times10^{-3}}$	2.4×10^{-3}	4.8×10^{-3}
18	α_L	longitudinal dispersivity coefficient	m	0.01	0.05	**0.1**	0.25	0.5
19	α_L/α_T	ratio. α_T = transversal dispersivity coeff.	–	1	5	**10**	15	20

HESSD
8, 7657–7707, 2011

Table 3. Summary of lens characteristics in seepage and infiltration areas derived from TEC-probe and ECPT measurements.

	Lens characteristic	Unit	TEC-probe Range	TEC-probe Median	TEC-probe No.	ECPT Range	ECPT Median	ECPT No.	TEC + ECPT Median
Seepage areas	D_{mix}	m b.g.l.	0.8–2.5	1.5	17	1.2–3.5	1.7	13	1.7
	B_{mix}	m b.g.l.	1.2–3.6	2.5	17	2.0–5.5	3.7	13	2.8
	W_{mix}	m	0.2–1.7	0.7	17	0.5–3.7	1.5	13	0.9
Infiltration areas	D_{mix}	m b.g.l.	>4.0	>4.0	10	4.0–11.0	6.3	9	
	B_{mix}	m b.g.l.	>4.0	>4.0	10	8.0–14.0	8.5	9	
	W_{mix}	m	?	?	10	1.0–5.5	3.0	9	

Maximum penetration depth of TEC-probe was 4 m b.g.l., penetration depth of ECPT was 25 m b.g.l.
D_{mix} = centre of mixing zone, B_{mix} = bottom of mixing zone, W_{mix} = half width of mixing zone (= $D_{mix} - B_{mix}$).

HESSD
8, 7657–7707, 2011

Shallow rainwater lenses in deltaic areas with saline seepage

P. G. B. de Louw et al.

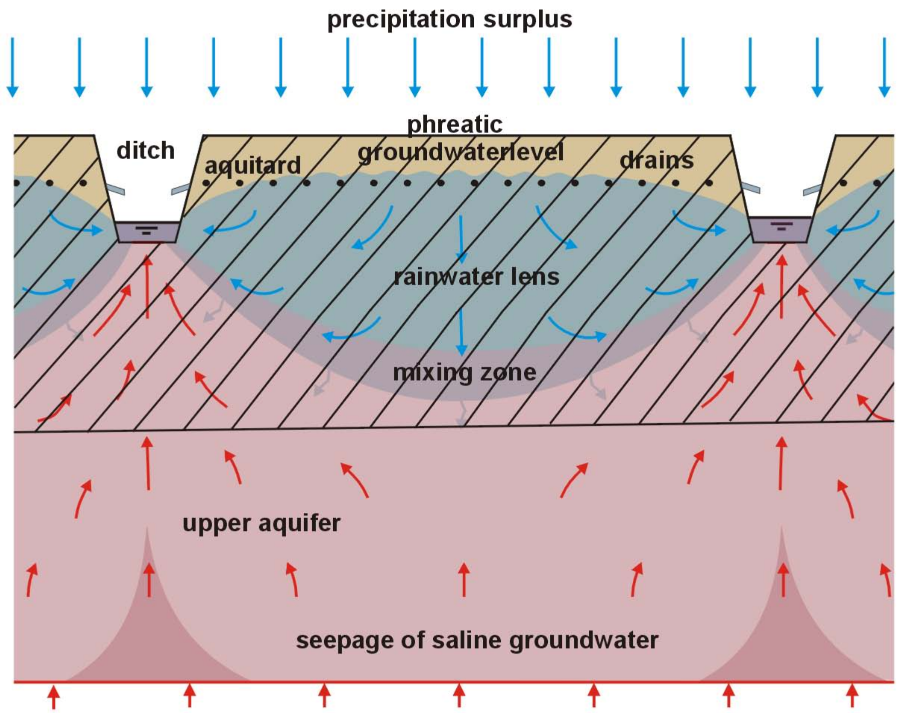

Fig. 1. Conceptual visualisation of a shallow rainwater lens on top of saline groundwater seepage.

HESSD
8, 7657–7707, 2011

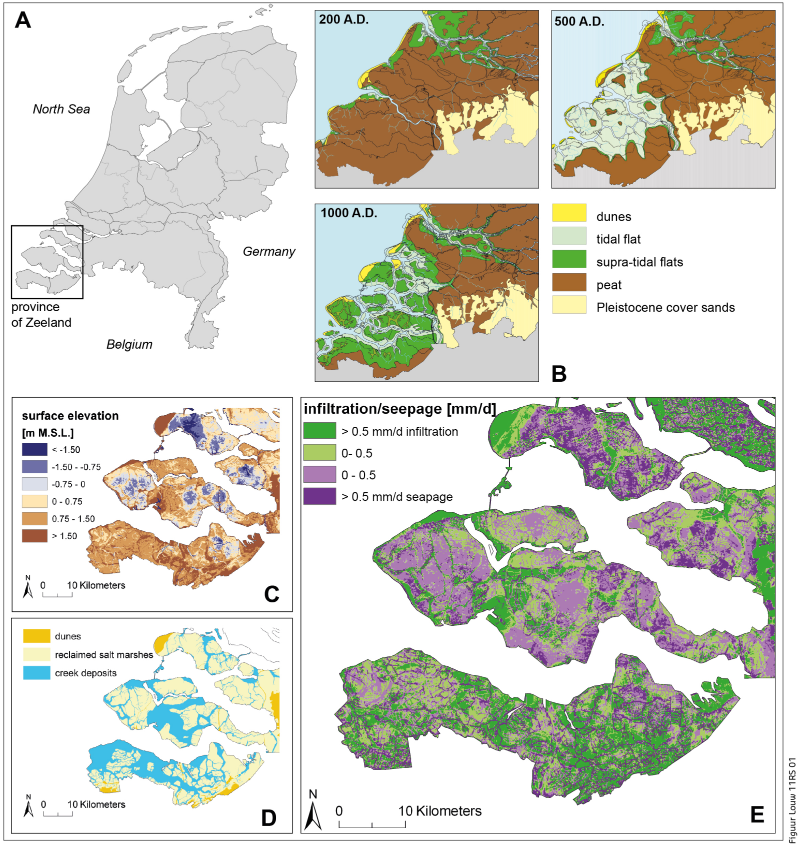

Fig. 2. **(a)** Location of study area. **(b)** Paleogeography of study area in 200 A.D., 500 A.D., 1000 A.D. (Vos and Zeiler, 2008; by courtesy of Vos). **(c)** Surface elevation. **(d)** Position of the dunes, reclaimed salt marshes and sandy creek deposits (from: REGIS II, 2005). **(e)** Infiltration and seepage flux (result of regional groundwater model; Van Baaren et al., 2011).

HESSD
8, 7657–7707, 2011

Shallow rainwater lenses in deltaic areas with saline seepage

P. G. B. de Louw et al.

Title Page
Abstract Introduction
Conclusions References
Tables Figures
◄ ►
◄ ►
Back Close
Full Screen / Esc
Printer-friendly Version
Interactive Discussion

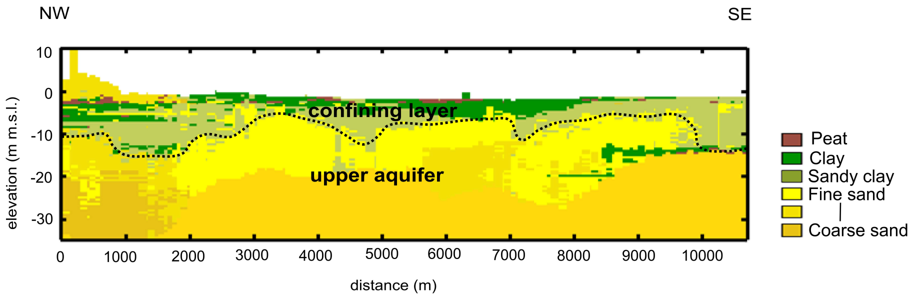

Fig. 3. A NW-SE lithological cross-section of the island of Schouwen-Duivenland (see Fig. 4 for location of cross-section). The cross-section is derived from a detailed 3-D geological model of Zeeland based on drillings (5 drillings per 1 km^2) that were classified into geological units (GeoTOP, Stafleu et al., 2011).

HESSD
8, 7657–7707, 2011

Shallow rainwater lenses in deltaic areas with saline seepage

P. G. B. de Louw et al.

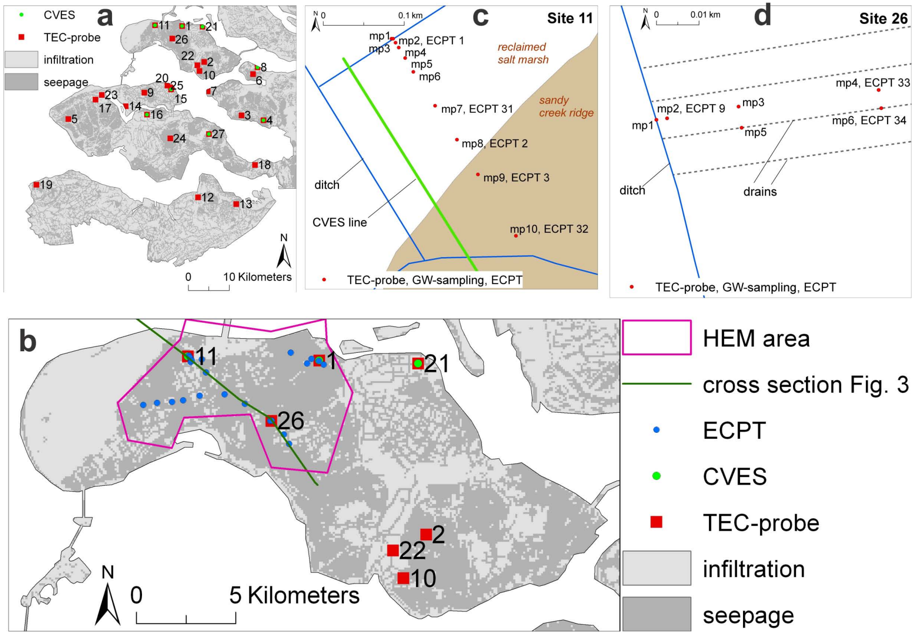

Fig. 4. Position of field measurements at different scales. **(a)** Province of Zeeland. **(b)** Island of Schouwen-Duivenland. **(c)** Agricultural field, site 11. **(d)** Agricultural field, site 26.

HESSD
8, 7657–7707, 2011

Shallow rainwater lenses in deltaic areas with saline seepage

P. G. B. de Louw et al.

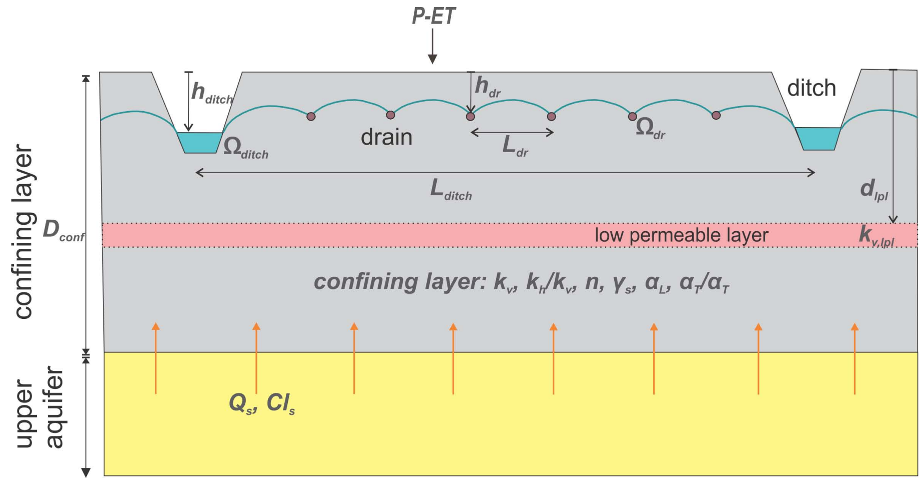

Fig. 5. Conceptual schematization of the cross-sectional 2-D-models.

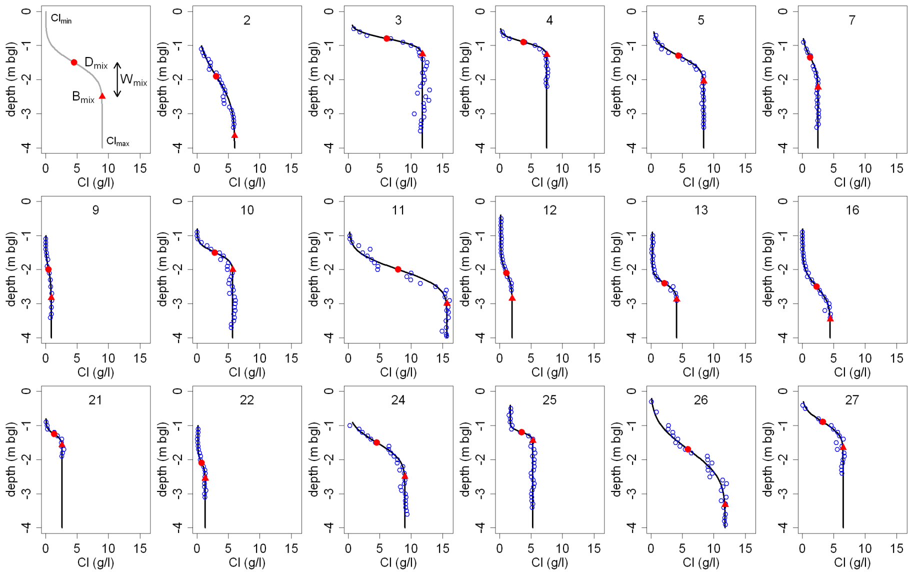

Fig. 6. Characteristics of a rainwater lens, D_{mix}, B_{mix}, W_{mix}, $\mathrm{Cl_{min}}$, $\mathrm{Cl_{max}}$ (first plot) and 17 measured salinity profiles with the TEC-probe (blue circles) at different seepage locations in the province of Zeeland (see Fig. 4a for TEC-probe locations). The measured salinity profiles are characterized by the fitted salinity profiles based on spatial moments (black line).

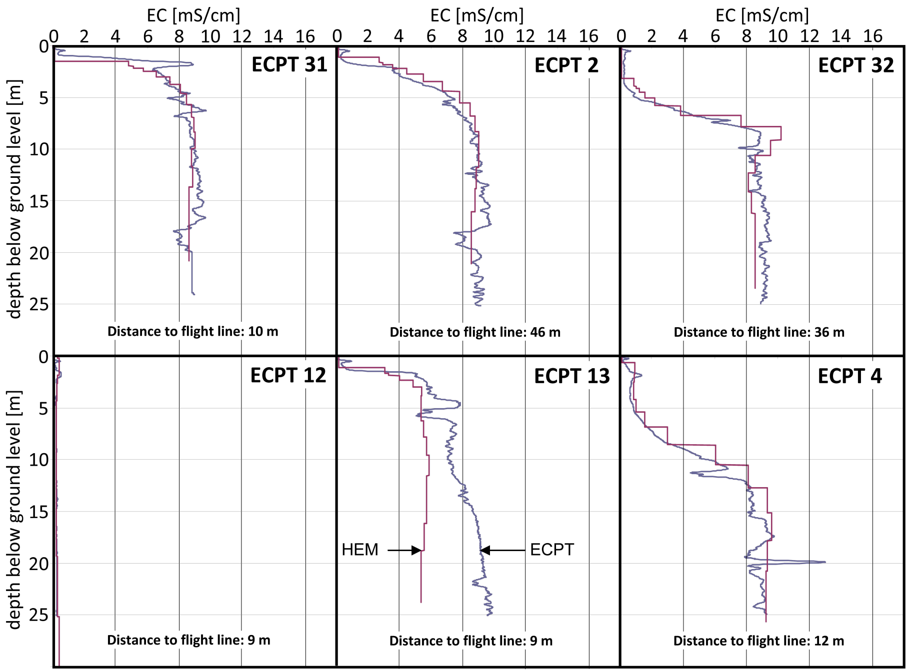

Fig. 7. Comparison of six ECPT soundings and smooth 15-layer HEM inversion models (for location see Fig. 14).

HESSD
8, 7657–7707, 2011

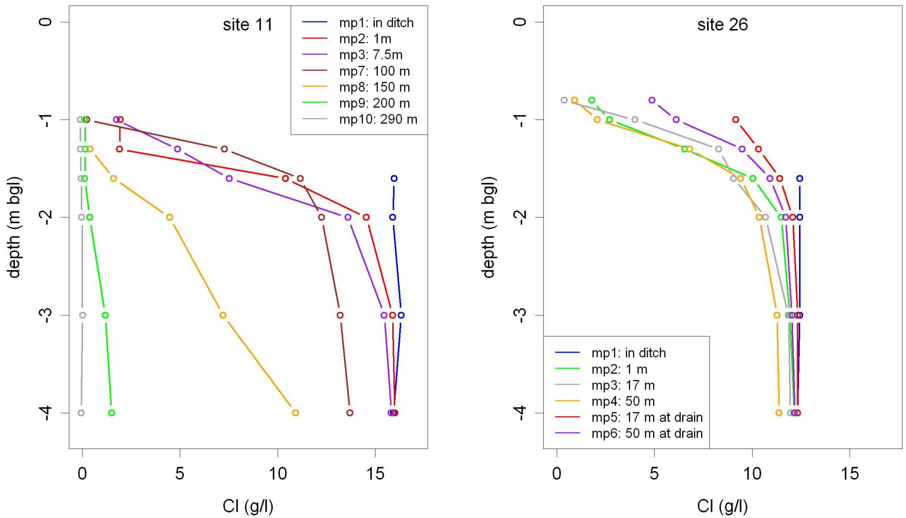

Fig. 8. Salinity profiles measured by groundwater sampling for sites 11 and 26 (on 21 January 2010).

HESSD
8, 7657–7707, 2011

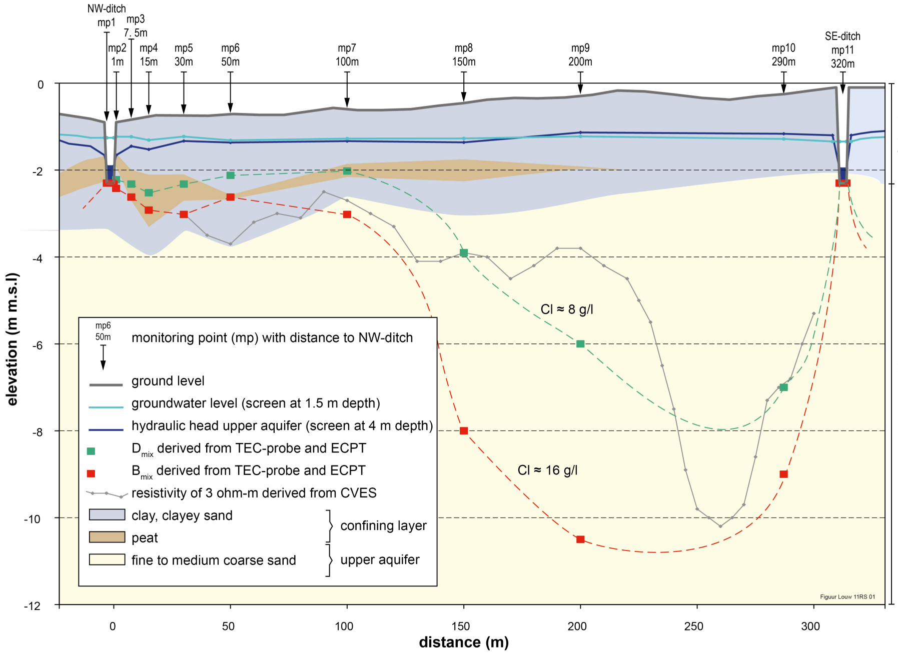

Fig. 9. Cross-section of site 11 with the measured hydraulic head at 1.5 m and 4 m depth, D_{mix} and B_{mix} derived from TEC-probe and ECPT, and the real inverted soil resistivity isoline of 3 Ωm derived from CVES measurements. Note that the CVES-line was situated about 60 m from the 1-D in situ measurements (Fig. 4c) and therefore shows a sharper gradient.

HESSD
8, 7657–7707, 2011

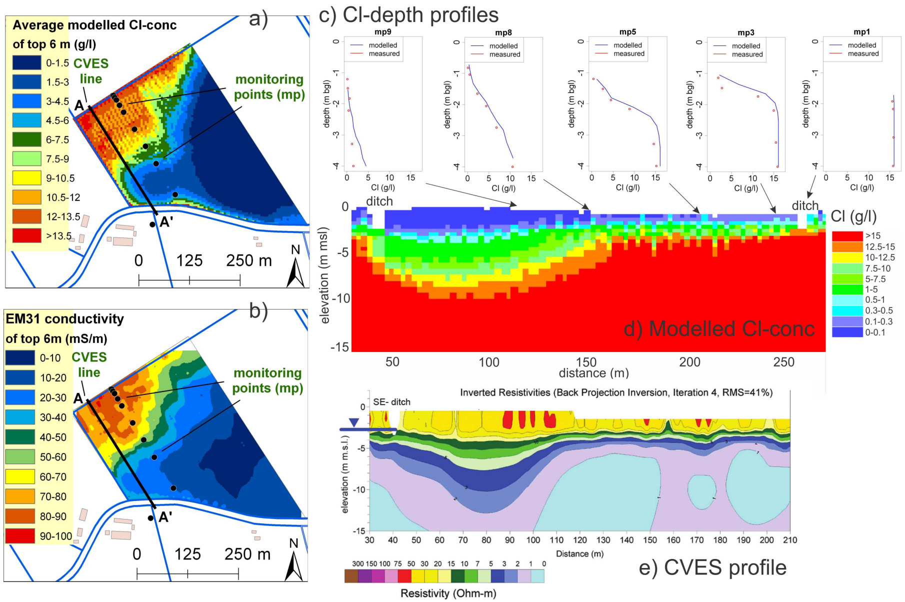

Fig. 10. Comparison of model results (3-D-model) with field measurements (EM13, Cl-depth profiles, CVES) for site 11.

HESSD
8, 7657–7707, 2011

Shallow rainwater lenses in deltaic areas with saline seepage

P. G. B. de Louw et al.

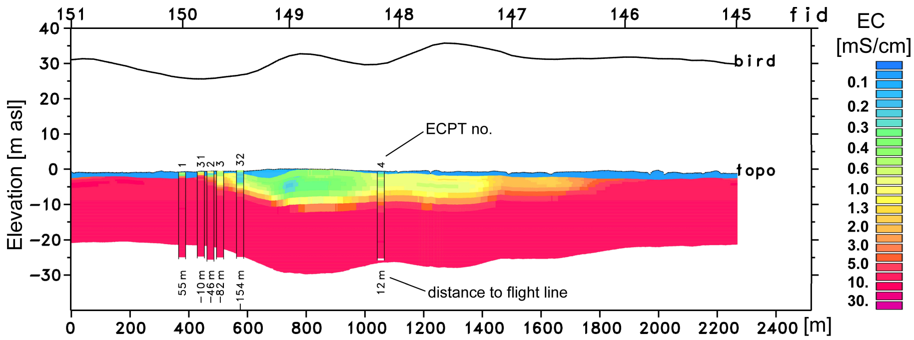

Fig. 11. Portion of flight line 9 (for location see Fig. 14) displaying smooth 15-layer HEM inversion models and nearby ECPT measurements.

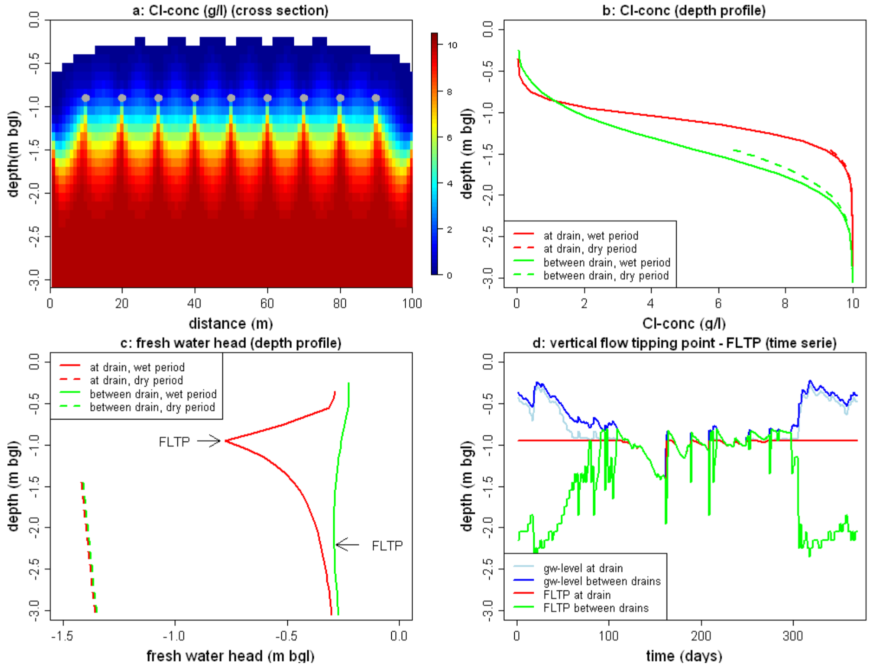

Fig. 12. Model results of the reference 2-D-conceptual model. **(a)** Cl-concentration in cross-section between two ditches (wet period). **(b)** Cl-conc. – depth profile for a location at and between drains (wet and dry period). **(c)** Fresh water head depth profile for location at and between drains (wet and dry period). **(d)** Time series of vertical flow tipping point (FLTP) and groundwater level for a location at and between drains.

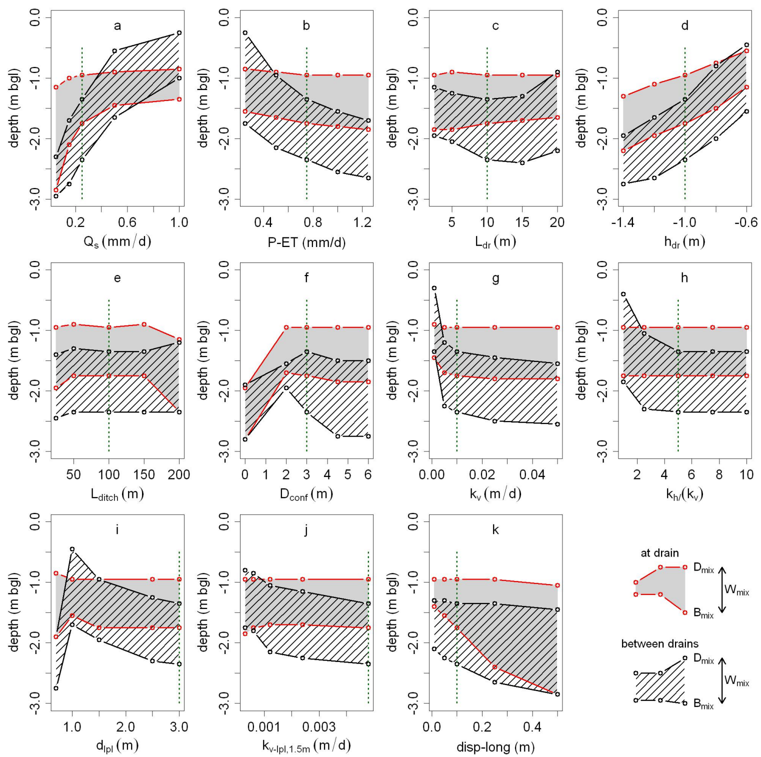

Fig. 13. Results of the sensitivity analysis for the 11 most sensitive parameters for lens characteristics D_{mix}, B_{mix} and W_{mix} (effect > 0.1 m). The x-axis gives the parameter values of the reference model and the four sensitivity models; the y-axis gives the position of D_{mix} and B_{mix} for the different models, for a location at a drain and between two drains. The green dotted line indicates the position of the reference model.

HESSD
8, 7657–7707, 2011

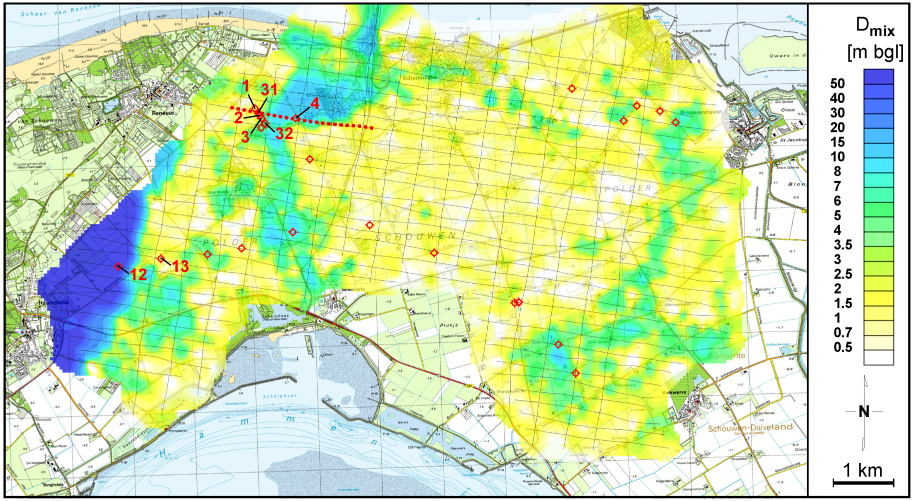

Fig. 14. Estimated depth D_{mix} (average position of the mixing zone in m below ground level) derived from HEM inversion models. All flight lines (black lines) as well as a portion of line 9 (red dots) and the location of the ECPTs (red circles, those shown in Figs. 7 and 11 are numbered) are plotted on top of the depth map.

HESSD
8, 7657–7707, 2011

Shallow rainwater lenses in deltaic areas with saline seepage

P. G. B. de Louw et al.

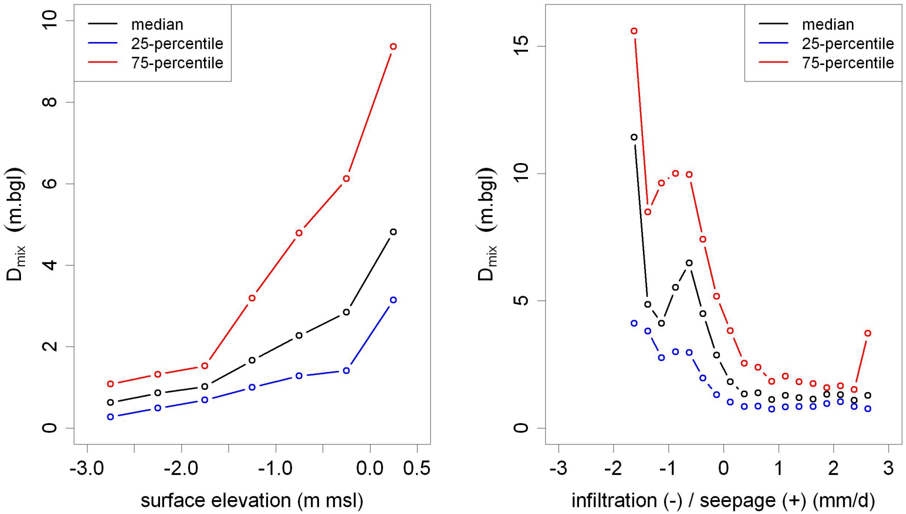

Fig. 15. Relation of D_{mix} derived from 84 300 HEM-measurements with **(a)** Surface elevation (m m.s.l.) and **(b)** Infiltration and seepage flux (mm d^{-1}). The 25-, 50- and 75-percentile of D_{mix} was determined and plotted for different classes of surface elevation and flux (dots represent middle of class).

HESSD
8, 7657–7707, 2011

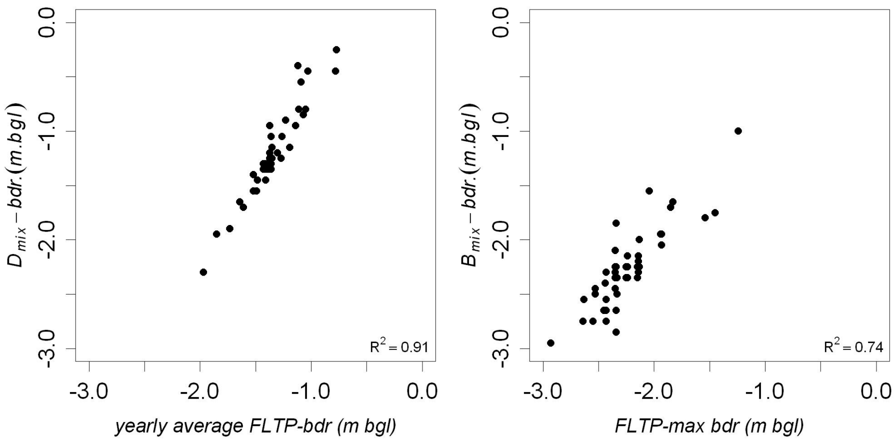

Fig. 16. Correlation scatter diagrams of calculated vertical flux tipping points (FLTP) and lens characteristics D_{mix} and B_{mix}. bdr = between drains.

HESSD
8, 7657–7707, 2011